nature portfolio

https://doi.org/10.1038/s41550-021-01581-z

Supplementary information

Titanium oxide and chemical inhomogeneity in the atmosphere of the exoplanet WASP-189 b

In the format provided by the authors and unedited

Date	#Spectra[a]	Exp. time [s]	Airmass[b]	SNR @ 550 nm[c]	Orbital Phase ϕ [d]
2018-03-26	39 (15/24)	600	1.97-1.11-1.52	144.6-213.2	0.99-0.096
2019-04-14	126 (69/57)	200	2.06-1.11-1.64	98.8-187.9	0.94-0.065
2019-04-25	107 (52/55)	200	1.56-1.11-2.06	97.7-176.0	0.98-0.087
2019-05-06	112 (69/43)	200	2.00-1.18-2.00	108.4-161.6	0.95-0.055
2019-05-14	122 (68/54)	200	1.94-1.11-2.27	90.0-136.1	0.93-0.047

Supplementary Table 1: Overview of the observations. [(a)] In parenthesis: spectra in- and out-of-transit, respectively. [(b)] Airmass at the beginning, the peak of the altitude, and end of observation. [(c)] Minimum and maximum SNR value at 550 nm. [(d)] Orbital phase at the start and end of the observation. The transit starts at $\phi = 0.967$ and ends at $\phi = 0.033$. The observations taken in the nights of 2018-03-26 and 2019-04-25 hence only partially cover transits.

	$v_{\mathrm{orb,proj}}$[km/s]	$v_{\mathrm{sys,p}}$[km/s]	$M_*[M_\odot]$
2018-03-26*	152.9 ± 7.6	-23.36 ± 0.67	–
2019-04-14	190.8 ± 5.3	-25.67 ± 0.25	1.96 ± 0.16
2019-04-25	196 ± 12	-28.58 ± 0.70	2.13 ± 0.40
2019-05-06	187.2 ± 6.4	-27.59 ± 0.32	1.86 ± 0.19
2019-05-14	202.6 ± 9.2	-27.14 ± 0.39	2.35 ± 0.32
Mean	194.1 ± 4.3	-27.2 ± 0.22	2.08 ± 0.14

Supplementary Table 2: Best-fit parameters for the orbital velocity, systemic velocity and the stellar mass for all five nights of observation. *: Due to long exposure times and only covering a half transit, this night of observations was not used to calculate the stellar mass and not taken into consideration when calculating the mean values. The best-fit orbital velocity (194.1 ± 4.3 km s^{-1}) is smaller than the calculated velocity using the parameters stated by Lendl et al. 2020[16], $v_{\mathrm{orb,p}} = v_{\mathrm{orb}} \sin i = \frac{2\pi a \sin i}{P} = 200.7 \pm 4.9\,\mathrm{km\,s^{-1}}$, which shows that the planet's atmosphere is moving at a different speed, hence shows effects of winds. The measured systemic velocity is marginally smaller than the true systemic velocity as measured by Anderson et al. 2018[14], which can be the result of day-to-night-side winds in the atmosphere of the exoplanet.

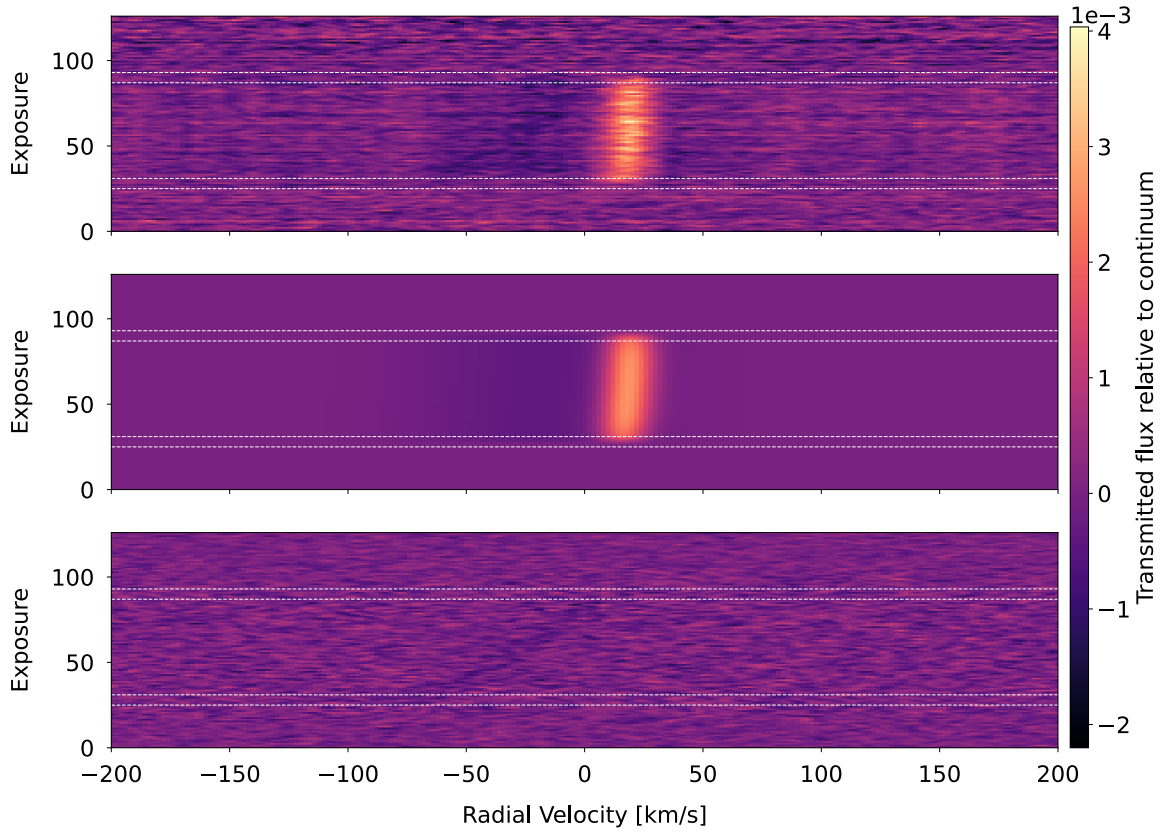

Supplementary Figure 1: Illustration of Doppler shadow subtraction and detrending of the cross-correlation function for the time-series observed on April 14, 2019, with the Fe^+ template at 4,000 K (see Methods). **Top panel:** Raw two-dimensional cross-correlation function. During the transit, the Doppler shadow emerges as the positive near-vertical structure. Time of first, second, third and fourth contact as predicted using the ephemeris of Lendl et al. (2020)[16] are indicated as dashed lines. **Middle panel:** Best-fit model of the Doppler shadow. **Bottom panel:** Residuals after subtracting the best-fit model from the raw cross-correlation function (top panel) and application of a detrending algorithm in the vertical direction. The absorption signature of the planet atmosphere is visible as the slanted feature, Doppler-shifted to the instantaneous radial velocity of the planet. The residual of the Doppler shadow at the end of the transit is masked during further analysis.

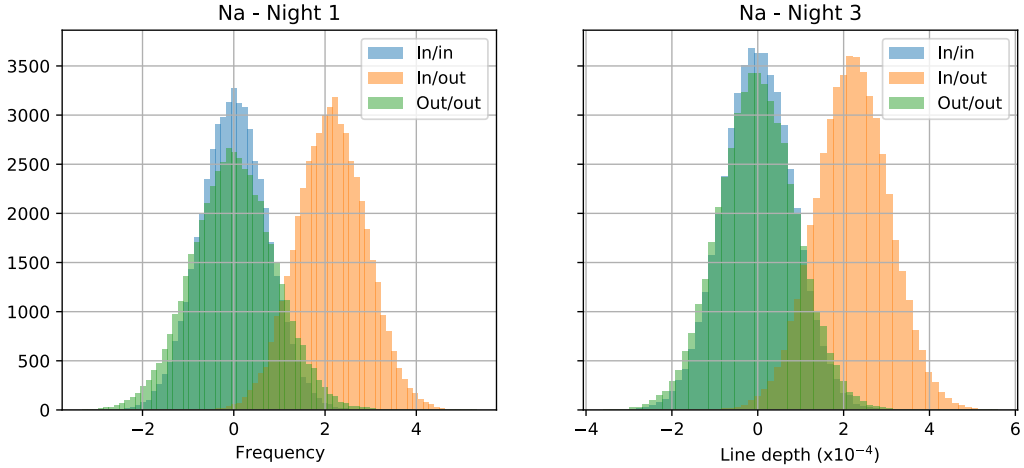

Supplementary Figure 2: The distributions of randomly generated instances of the one-dimensional cross-correlation function at the rest-frame velocity of the planet for the Na doublet, for each of the two nights in which the transit was fully covered. The in- and out-of-transit master functions are constructed by taking random subsets of the in-, resp. out-of-transit exposures. The measured line depth is expected to be around zero for out-out (in green) and in-in (in blue), i.e. where the randomly picked subset is normalised (subtracted) with its own master-spectrum. Only when the in-transit cross-correlation functions are normalised by the out-of-transit master spectrum (in-out, in orange), we expect the measured line amplitude to be different from zero.

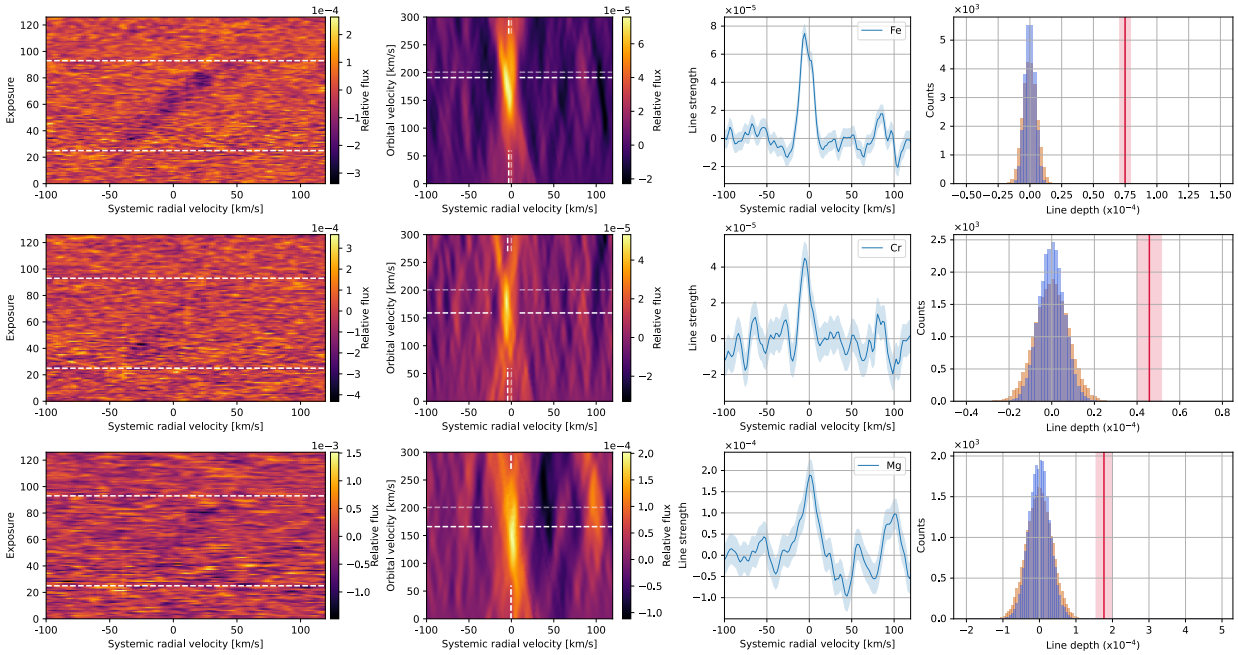

Supplementary Figure 3: Bootstrap results for Fe, Cr and Mg. **First and second column:** Two-dimensional exposure-velocity maps and cross-correlation functions in $K_\mathrm{p} - V_\mathrm{sys}$ space in the rest frame of the star. **Third column:** All cross-correlation functions co-added in the rest-frame of the planet shifted to the rest frame of the star, assuming orbital velocities as given in Table 1(indicated by the strong dashed line in the second column of panels) to account for the apparent shifts due to morning-to-evening limb asymmetries. The blue-shaded area indicates the 1σ uncertainty interval as determined through Gaussian error propagation of the expected photon noise on the individual spectra. **Forth column:** Distributions of Gaussian fits to random realisations of the one-dimensional cross-correlation function generated by stacking the time-series of cross-correlation functions with random Doppler shifts. Gaussian functions are fitted with fixed widths of $10\,\mathrm{km\,s^{-1}}$ (in orange) and $20\,\mathrm{km\,s^{-1}}$ (in blue). These widths correspond to typical widths observed in the real detections. These distributions are used to illustrate the robustness of the detections of each species, given the real and possibly correlated noise properties of the cross-correlation functions. The orange ($10\,\mathrm{km\,s^{-1}}$) distributions are wider than the blue ($20\,\mathrm{km\,s^{-1}}$) distributions. This is because systematic fluctuations that are wider are less likely to occur randomly. The red lines indicate the line depths of the detected species, and the red-shaded area the corresponding 1σ uncertainty.

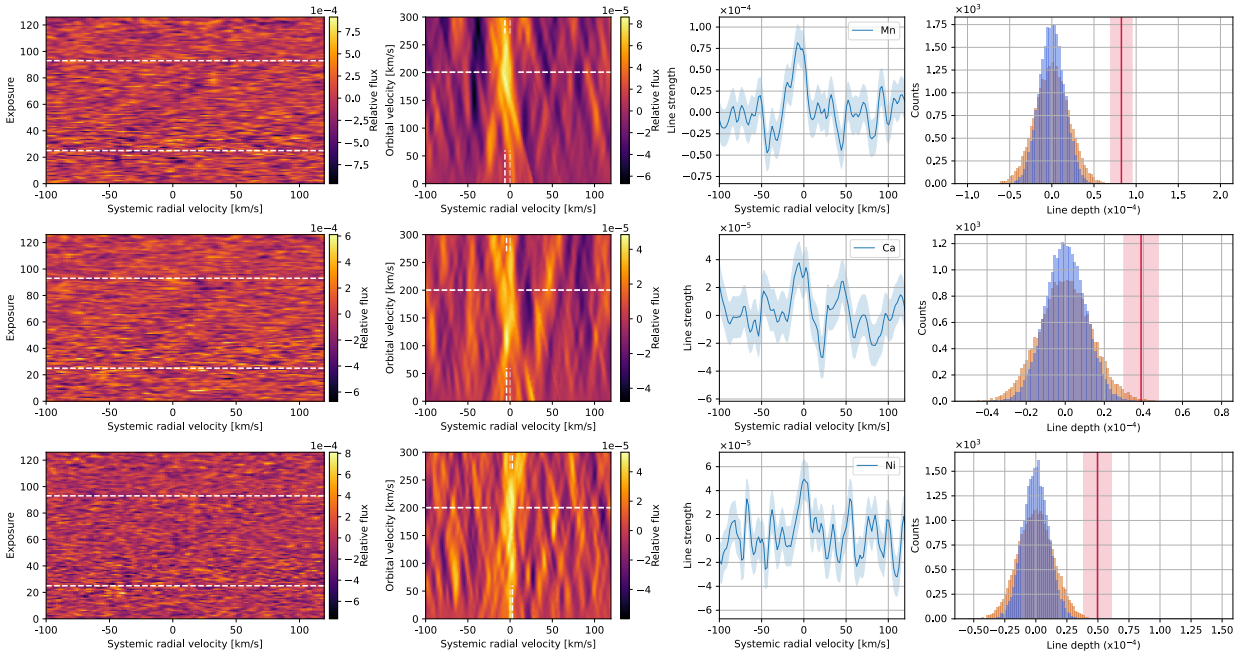

Supplementary Figure 4: Bootstrap results for Mn, Ca and Ni. **First and second column:** Two-dimensional exposure-velocity maps and cross-correlation functions in $K_\mathrm{p} - V_\mathrm{sys}$ space in the rest frame of the star. **Third column:** All cross-correlation functions co-added in the rest-frame of the planet shifted to the rest frame of the star, assuming orbital velocities as given in Table 1 (indicated by the strong dashed line in the second column of panels) to account for the apparent shifts due to morning-to-evening limb asymmetries. The blue-shaded area indicates the 1σ uncertainty interval as determined through Gaussian error propagation of the expected photon noise on the individual spectra. **Forth column:** Distributions of Gaussian fits to random realisations of the one-dimensional cross-correlation function generated by stacking the time-series of cross-correlation functions with random Doppler shifts. Gaussian functions are fitted with fixed widths of $10\,\mathrm{km\,s^{-1}}$ (in orange) and $20\,\mathrm{km\,s^{-1}}$ (in blue). These widths correspond to typical widths observed in the real detections. These distributions are used to illustrate the robustness of the detections of each species, given the real and possibly correlated noise properties of the cross-correlation functions. The orange ($10\,\mathrm{km\,s^{-1}}$) distributions are wider than the blue ($20\,\mathrm{km\,s^{-1}}$) distributions. This is because systematic fluctuations that are wider are less likely to occur randomly. The red lines indicate the line depths of the detected species, and the red-shaded area the corresponding 1σ uncertainty.

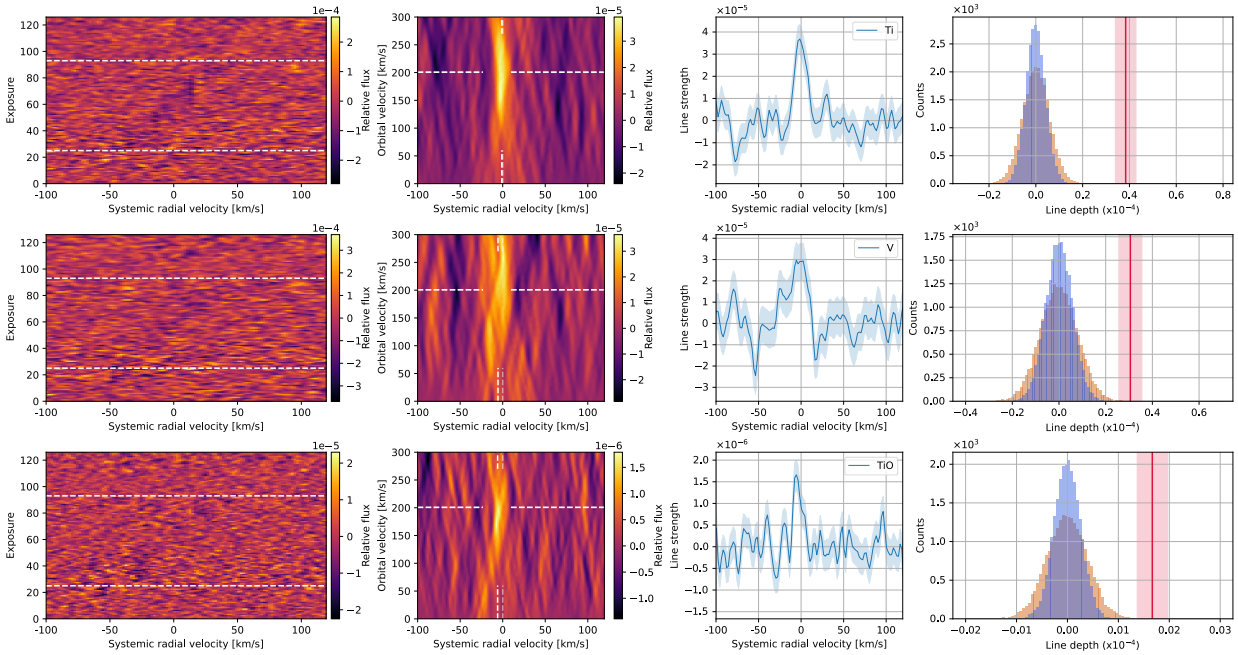

Supplementary Figure 5: Bootstrap results for Ti, V, and TiO. **First and second column:** Two-dimensional exposure-velocity maps and cross-correlation functions in $K_\mathrm{p} - V_\mathrm{sys}$ space in the rest frame of the star. **Third column:** All cross-correlation functions co-added in the rest-frame of the planet shifted to the rest frame of the star, assuming orbital velocities as given in Table 1 (indicated by the strong dashed line in the second column of panels) to account for the apparent shifts due to morning-to-evening limb asymmetries. The blue-shaded area indicates the 1σ uncertainty interval as determined through Gaussian error propagation of the expected photon noise on the individual spectra. **Forth column:** Distributions of Gaussian fits to random realisations of the one-dimensional cross-correlation function generated by stacking the time-series of cross-correlation functions with random Doppler shifts. Gaussian functions are fitted with fixed widths of $10\,\mathrm{km\,s^{-1}}$ (in orange) and $20\,\mathrm{km\,s^{-1}}$ (in blue). These widths correspond to typical widths observed in the real detections. These distributions are used to illustrate the robustness of the detections of each species, given the real and possibly correlated noise properties of the cross-correlation functions. The orange ($10\,\mathrm{km\,s^{-1}}$) distributions are wider than the blue ($20\,\mathrm{km\,s^{-1}}$) distributions. This is because systematic fluctuations that are wider are less likely to occur randomly. The red lines indicate the line depths of the detected species, and the red-shaded area the corresponding 1σ uncertainty.

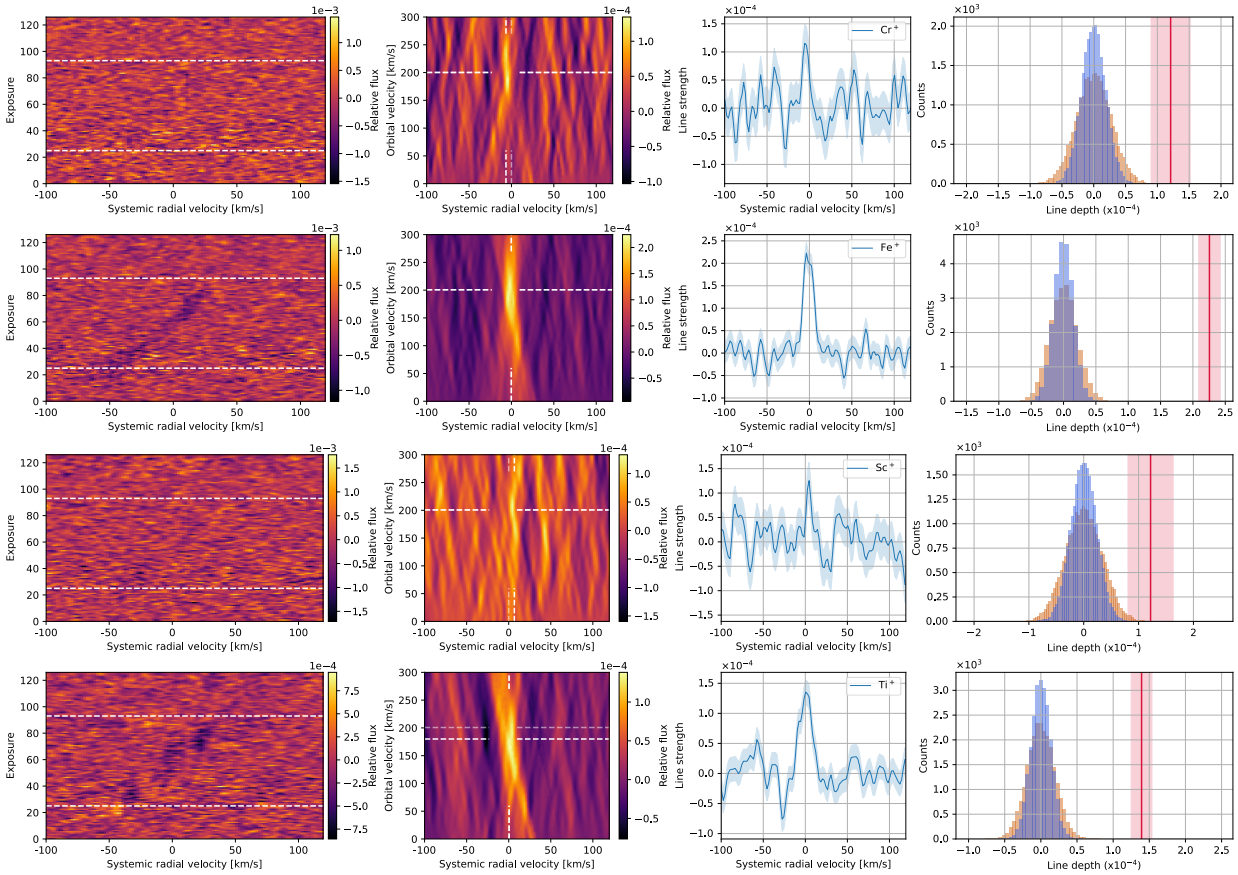

Supplementary Figure 6: Bootstrap results for Cr^+, Fe^+, Sc^+ and Ti^+. **First and second column:** Two-dimensional exposure-velocity maps and cross-correlation functions in $K_p - V_{sys}$ space in the rest frame of the star. **Third column:** All cross-correlation functions co-added in the rest-frame of the planet shifted to the rest frame of the star, assuming orbital velocities as given in Table 1 (indicated by the strong dashed line in the second column of panels) to account for the apparent shifts due to morning-to-evening limb asymmetries. The blue-shaded area indicates the 1σ uncertainty interval as determined through Gaussian error propagation of the expected photon noise on the individual spectra. **Forth column:** Distributions of Gaussian fits to random realisations of the one-dimensional cross-correlation function generated by stacking the time-series of cross-correlation functions with random Doppler shifts. Gaussian functions are fitted with fixed widths of $10\,\mathrm{km\,s^{-1}}$ (in orange) and $20\,\mathrm{km\,s^{-1}}$ (in blue). These widths correspond to typical widths observed in the real detections. These distributions are used to illustrate the robustness of the detections of each species, given the real and possibly correlated noise properties of the cross-correlation functions. The orange ($10\,\mathrm{km\,s^{-1}}$) distributions are wider than the blue ($20\,\mathrm{km\,s^{-1}}$) distributions. This is because systematic fluctuations that are wider are less likely to occur randomly. The red lines indicate the line depths of the detected species, and the red-shaded area the corresponding 1σ uncertainty.

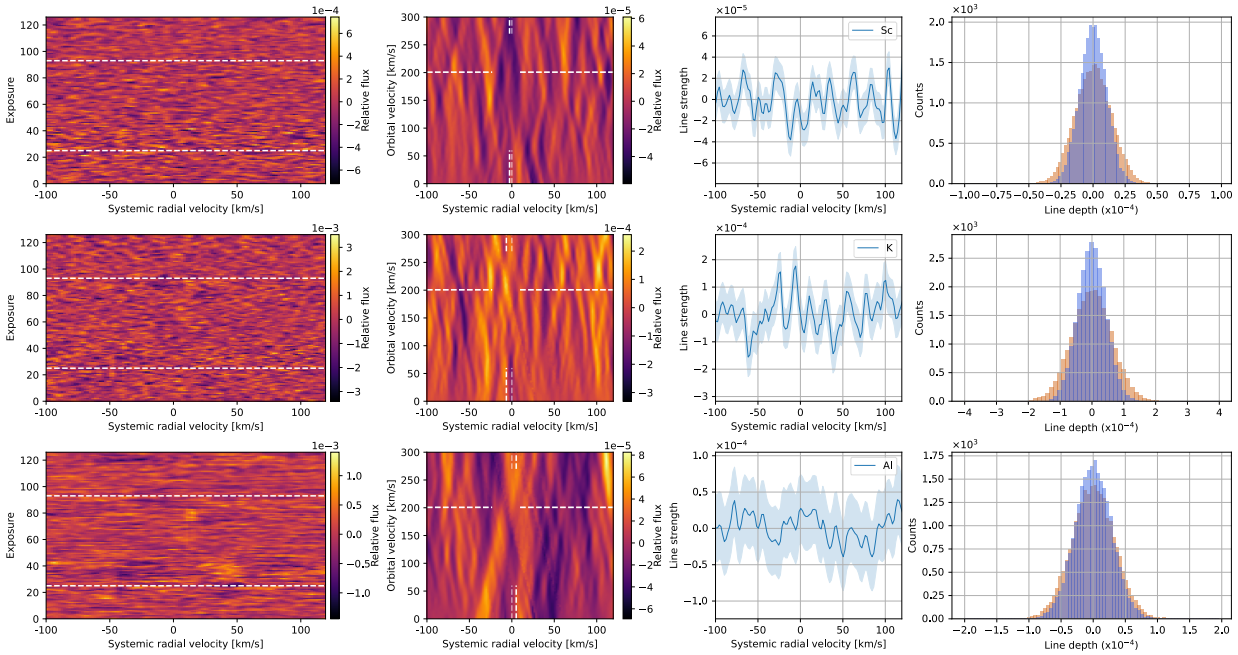

Supplementary Figure 7: Bootstrap results for Sc, K and Al. **First and second column:** Two-dimensional exposure-velocity maps and cross-correlation functions in $K_\mathrm{p} - V_\mathrm{sys}$ space in the rest frame of the star. **Third column:** All cross-correlation functions co-added in the rest-frame of the planet shifted to the rest frame of the star, assuming orbital velocities as given in Table 1 (indicated by the strong dashed line in the second column of panels) to account for the apparent shifts due to morning-to-evening limb asymmetries. The blue-shaded area indicates the 1σ uncertainty interval as determined through Gaussian error propagation of the expected photon noise on the individual spectra. **Forth column:** Distributions of Gaussian fits to random realisations of the one-dimensional cross-correlation function generated by stacking the time-series of cross-correlation functions with random Doppler shifts. Gaussian functions are fitted with fixed widths of $10\,\mathrm{km\,s^{-1}}$ (in orange) and $20\,\mathrm{km\,s^{-1}}$ (in blue). These widths correspond to typical widths observed in the real detections. These distributions are used to illustrate the robustness of the detections of each species, given the real and possibly correlated noise properties of the cross-correlation functions. The orange ($10\,\mathrm{km\,s^{-1}}$) distributions are wider than the blue ($20\,\mathrm{km\,s^{-1}}$) distributions. This is because systematic fluctuations that are wider are less likely to occur randomly.

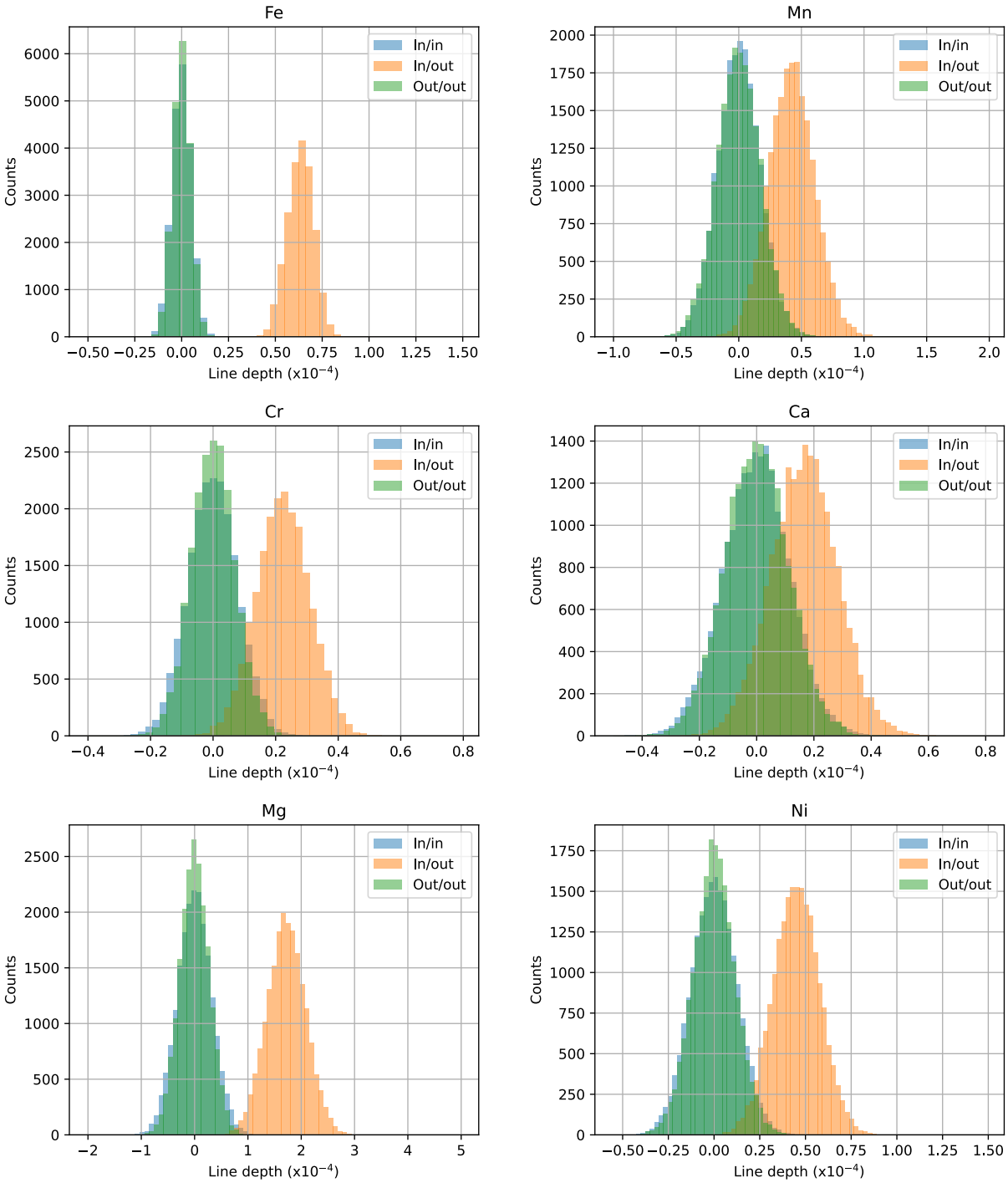

Supplementary Figure 8: The distributions of randomly generated instances of the one-dimensional cross-correlation function for Fe, Cr, Mg, Mn, Ca, and Ni at the rest-frame velocity of the planet. The in- and out-of-transit master functions are constructed by taking random subsets of the in-, resp. out-of-transit exposures. The measured line depth is expected to be around zero for out-out (in green) and in-in (in blue), i.e. where the randomly picked subset is normalised (subtracted) with its own master-spectrum. Only when the in-transit cross-correlation functions are normalised by the out-of-transit master spectrum (in-out, in orange), we expect the measured line amplitude to be different from zero.

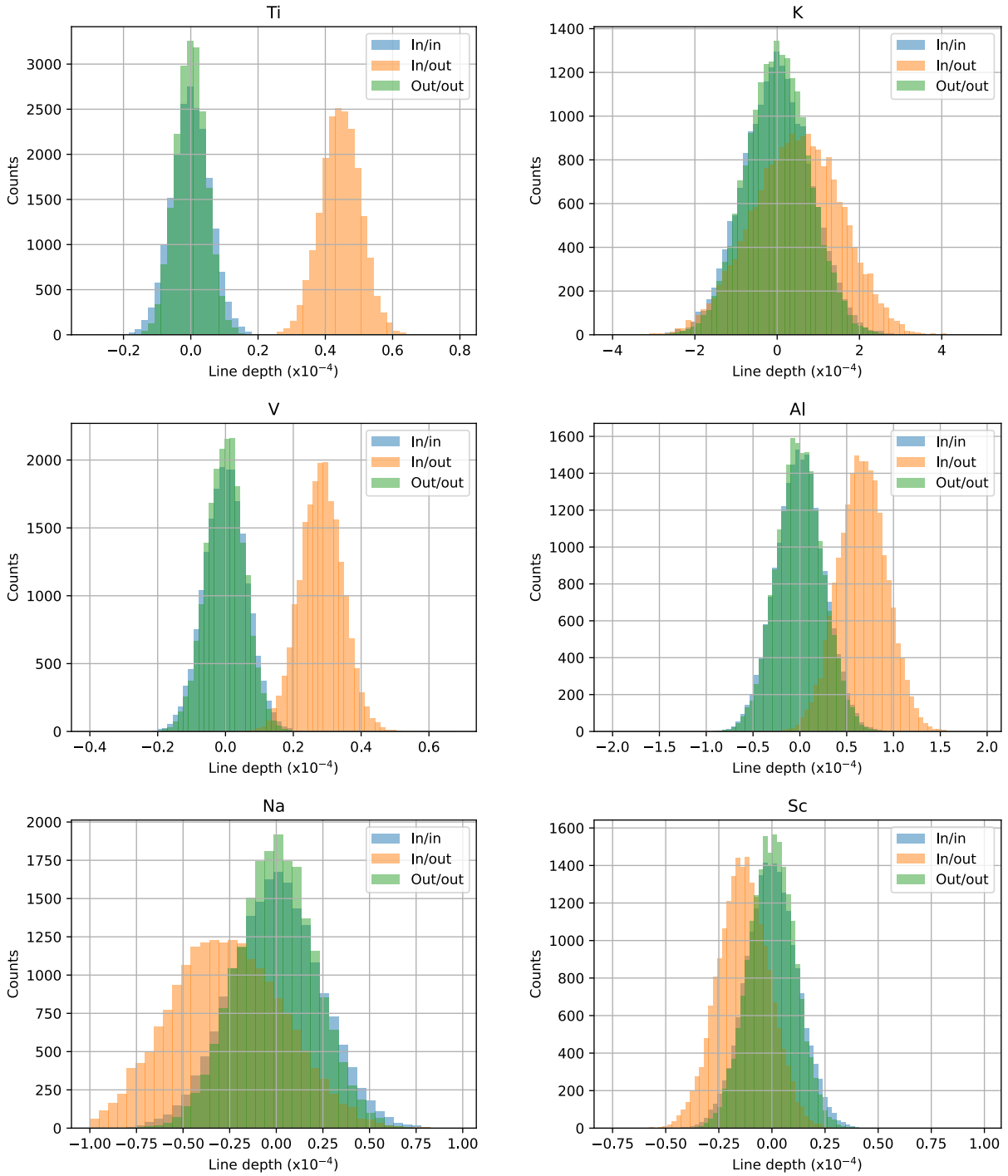

Supplementary Figure 9: The distributions of randomly generated instances of the one-dimensional cross-correlation function for Ti, V, Na, K, Al and Sc at the rest-frame velocity of the planet. The in- and out-of-transit master functions are constructed by taking random subsets of the in-, resp. out-of-transit exposures. The measured line depth is expected to be around zero for out-out (in green) and in-in (in blue), i.e. where the randomly picked subset is normalised (subtracted) with its own master-spectrum. Only when the in-transit cross-correlation functions are normalised by the out-of-transit master spectrum (in-out, in orange), we expect the measured line amplitude to be different from zero. Al seemingly presents a detection using this bootstrap method, but comparing to Supplementary Fig. 7 shows that there is no signal present in the $K_\mathrm{p} - V_\mathrm{sys}$ diagram.

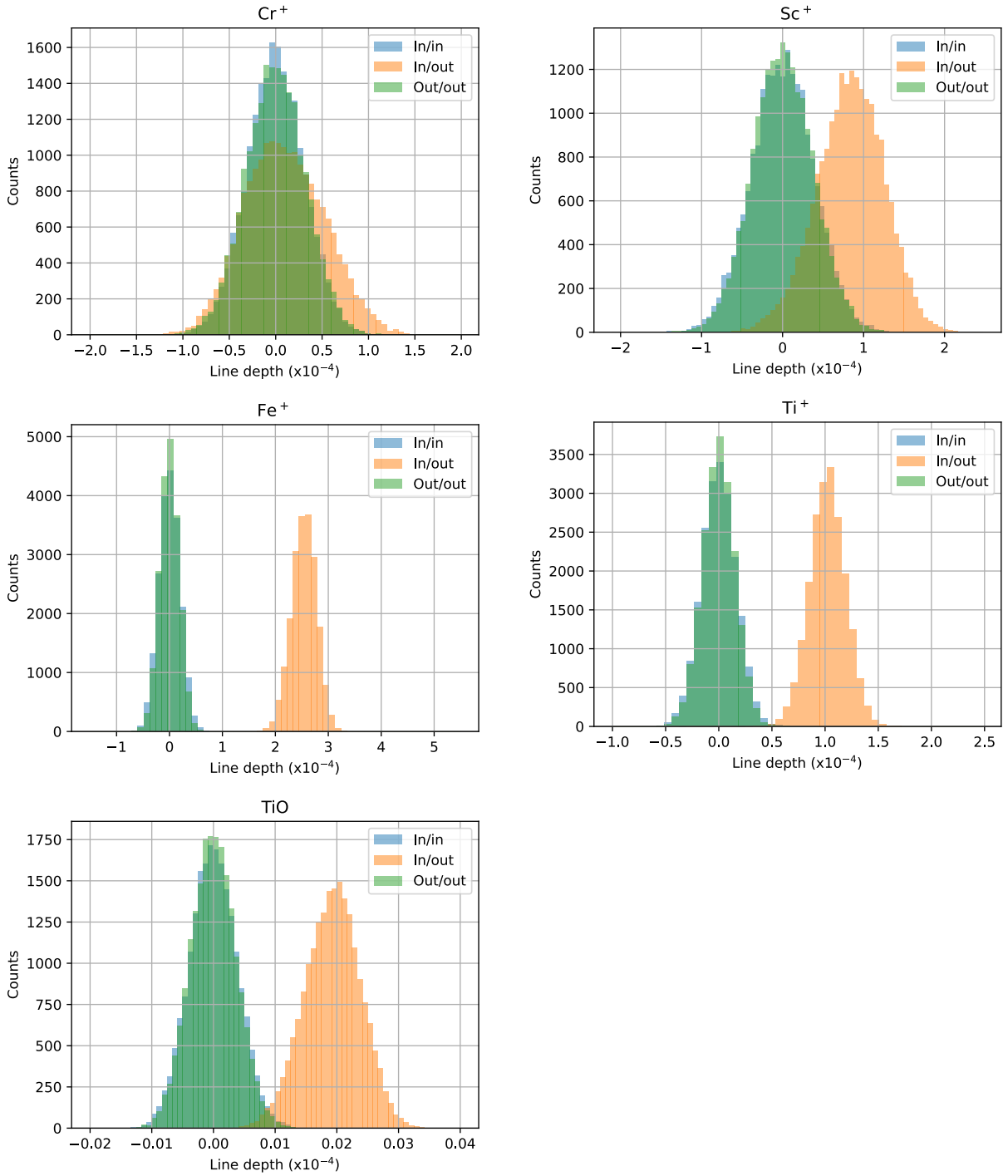

Supplementary Figure 10: The distributions of randomly generated instances of the one-dimensional cross-correlation function for Cr^+, Fe^+, TiO, Sc^+ and Ti^+ at the rest-frame velocity of the planet. The in- and out-of-transit master functions are constructed by taking random subsets of the in-, resp. out-of-transit exposures. The measured line depth is expected to be around zero for out-out (in green) and in-in (in blue), i.e. where the randomly picked subset is normalised (subtracted) with its own master-spectrum. Only when the in-transit cross-correlation functions are normalised by the out-of-transit master spectrum (in-out, in orange), we expect the measured line amplitude to be different from zero.